

Electronic Supplementary Information

Synthesis, structures and hydrogen storage properties of two new H-enriched compounds: $\text{Mg}(\text{BH}_4)_2(\text{NH}_3\text{BH}_3)_2$ and $\text{Mg}(\text{BH}_4)_2 \cdot (\text{NH}_3)_2(\text{NH}_3\text{BH}_3)$

Xiaowei Chen,^a ‡ Feng Yuan,^a ‡ Qinfen Gu,^b and Xuebin Yu *^a

^a Department of Materials Science, Fudan University, Shanghai 200433, China

^b Australian Synchrotron, Clayton, Victoria 3168, Australia

Author Contributions †These authors contributed equally to this work.

* To whom correspondence should be addressed. Phone and Fax: +86-21-5566 4581.

E-mail: yuxuebin@fudan.edu.cn

Experimental sections

Reagents and synthesis

$\text{Mg}(\text{BH}_4)_2$ was synthesized from MgCl_2 (99.9% purity, Sigma) and NaBH_4 (95% purity, Sigma) in dried diethyl ether as described in reference.¹ $\text{Mg}(\text{BH}_4)_2 \cdot 2\text{NH}_3$ was obtained by the reaction of NH_3 with $\text{Mg}(\text{BH}_4)_2$, following with heat treatment at 118 °C in a vacuum for 4h, according to previous report.² Ammonia borane (NH_3BH_3 , AB) (97% purity) were purchased from Sigma-Aldrich and used as-received form without further purification.

For the preparation of the $\text{Mg}(\text{BH}_4)_2\text{-2AB}$ and $\text{Mg}(\text{BH}_4)_2 \cdot 2\text{NH}_3\text{-AB}$ composites, approximately 0.3 g of mixtures of $\text{Mg}(\text{BH}_4)_2$ and AB with mole ratios of 1 : 2, and mixtures of $\text{Mg}(\text{BH}_4)_2 \cdot 2\text{NH}_3$ and AB with mole ratios of 1 : 1 were ball milled using a QM-3SP2 planetary ball mill at 260 rpm for 4 h in a 100 ml hardened steel bowl. The mass ratio of the sample to steel balls is 1:30. All sample handling was done in an argon-filled glove box equipped with a recirculation system to keep the H_2O and O_2 levels below 1 ppm.

Instrumentation and analyses

Hydrogen release property measurements were performed by thermogravimetry thermal analysis (TG, STA 449 C) connected to a mass spectrometer (MS, QMS 403) using a heating rate of 5 °C/min under a 1 atm N_2 atmosphere. Typical sample quantities were 5–10 mg, which is sufficient for getting accurate results due to the high sensitivity of the employed equipment. Temperature-programmed desorption (TPD) was also performed to determine the decomposition behavior of the sample on a semi-automatic Sievert's apparatus, connected with a reactor filled with sample (~0.1 g) under an argon atmosphere (1 bar) at a heating rate of 5 °C/min.

High-resolution synchrotron X-ray powder diffraction data were collected on the Powder Diffraction Beamline, Australian Synchrotron by using a Mythen-II detector. For phase identification, samples were loaded into pre-dried 0.7 mm glass capillary tubes inside the argon atmosphere glove box and sealed with vacuum grease for X-ray diffraction measurements. $\text{Mg}(\text{BH}_4)_2\text{-2AB}$ was indexed as having an orthorhombic lattice using program DICVOL06³ and space group $P2_12_12_1$ was assigned based on systematic absence analysis. The $\text{Mg}(\text{BH}_4)_2 \cdot 2\text{NH}_3\text{-AB}$ crystallizes in a tetragonal cell with space group $P4bm$. The structure solution was started using the powder charge-flipping algorithm (pCF) implemented in the program Superflip.⁴ Mg atoms were easily located in the electron density maps. However it was difficult to locate BH_4 and NH_3 .

molecules. The crystal structures were then identified using the direct space method in which the BH_4 and NH_3 , NH_3BH_3 units were input as rigid bodies with common bond lengths and bond angles in TOPAS.⁵ Rietveld refinement was performed using TOPAS⁵ and the refined lattice parameters are $a = 14.4135(2)$ Å, $b = 13.2084(2)$ Å and $c = 5.1118(1)$ Å for $\text{Mg}(\text{BH}_4)_2\cdot 2\text{AB}$, and $a = 9.4643(8)$ Å and $c = 5.5229(8)$ Å for $\text{Mg}(\text{BH}_4)_2\cdot 2\text{NH}_3\text{-AB}$. The Rietveld fit is excellent and consistent with the experimental X-ray profile, yielding the agreement factors of $R_{wp} = 4.5\%$, $R_B = 2.9\%$ and $\text{GoF} = 1.965$ for $\text{Mg}(\text{BH}_4)_2\cdot 2\text{AB}$, and $R_{wp} = 5.6\%$, $R_B = 4.1\%$ and $\text{GoF} = 2.136$ for $\text{Mg}(\text{BH}_4)_2\cdot 2\text{NH}_3\text{-AB}$.

Fourier transform infrared (FTIR) (Magna-IR 550 II, Nicolet) analyses were conducted to confirm the chemical bonds in the sample. Products were pressed with KBr and then loaded in a sealed chamber for the measurement.

The solid-state nuclear magnetic resonance (NMR) spectra were measured using a Bruker Avance 300 MHz spectrometer, using a Doty CP-MAS probe with no probe background. The powder samples collected after the decomposition reaction were spun at 5 kHz using 4 mm ZrO_2 rotors filled up in purified argon atmosphere glove boxes. A 0.55 ms single-pulse excitation was employed, with repetition times of 1.5 s.

Computational Details

First-principles calculations based on density-functional theory (DFT) were performed by using Vienna ab initio simulation package (VASP)⁶ with the projector-augmented wave scheme⁷ and the generalized-gradient approximation of Perdew-Burke-Ernzerhof^{8, 9} for the electronic exchange-correlation functional. The energy cut-off for the plane wave expansion was set to 400 eV to ensure sufficient convergence (less than 1 meV/cell). In the k-point sampling routine, $2\times 2\times 5$ and $3\times 3\times 5$ Monkhorst-Pack mesh¹⁰ were used for unit cell of $\text{Mg}(\text{BH}_4)_2\cdot 2\text{AB}$ and $\text{Mg}(\text{BH}_4)_2\cdot 2\text{NH}_3\text{-AB}$, respectively. Tests showed that our choice of k points yielded energies that converged within 0.01 eV/(f.u.). Since DFT methods have proven inadequate for describing weakly interacting systems due to their not accounting correctly for the ubiquitous van der Waals (vdW) forces, the DFT-D2 approach,¹¹ which adds a semiempirical pairwise force field to the conventional DFT calculations, was used to optimize the crystal structures of $\text{Mg}(\text{BH}_4)_2\cdot 2\text{AB}$ and $\text{Mg}(\text{BH}_4)_2\cdot 2\text{NH}_3\text{-AB}$. The geometric optimization was performed using fixed lattice constants, while atomic positions of Mg, B, N and H in the unit cell were allowed to relax until the residual

forces were less than $0.03 \text{ eV}\cdot\text{\AA}^{-1}$. To investigate the dehydrogenation dynamics for $\text{Mg}(\text{BH}_4)_2\cdot 2\text{AB}$ and $\text{Mg}(\text{BH}_4)_2\cdot 2\text{NH}_3\cdot\text{AB}$, we calculated the corresponding energy barriers by using the CI-NEB method.¹²

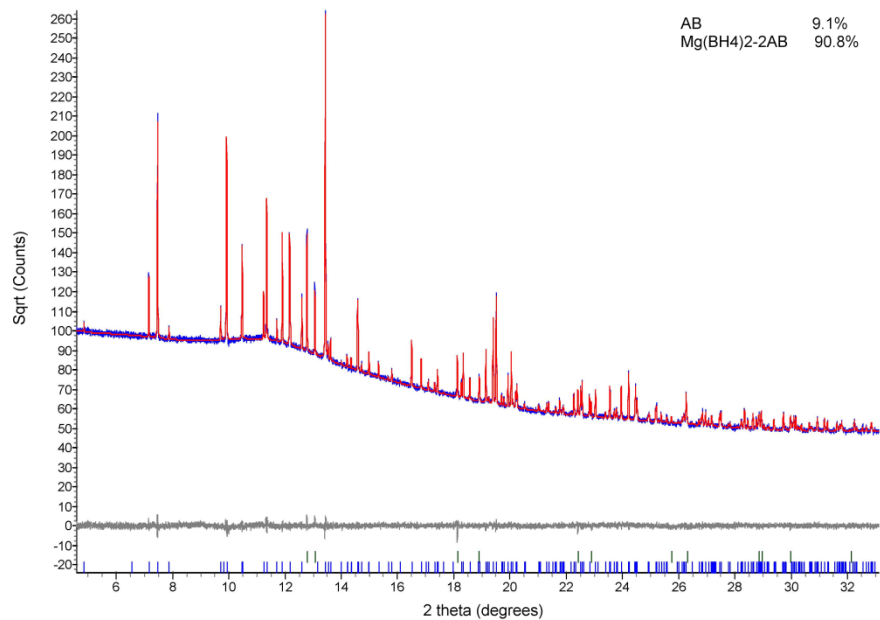


Fig. S1 Experimental (blue), fitted (red), and difference (line below observed and calculated patterns) synchrotron XRD profiles for Mg(BH₄)₂·2AB at 298 K. Vertical bars indicate the calculated positions of Bragg peaks for Mg(BH₄)₂·2AB and AB phases ($\lambda=0.8253\text{ \AA}$).

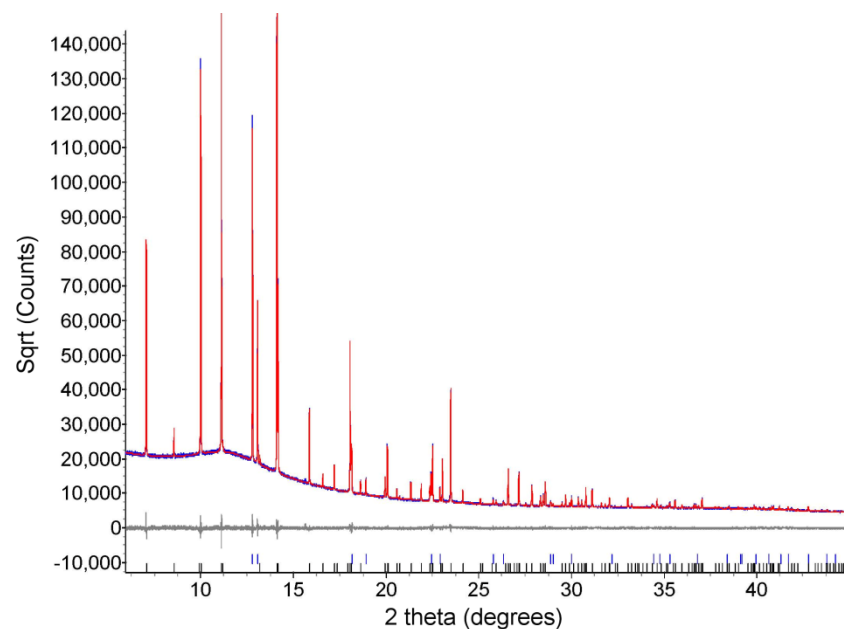


Fig. S2 Experimental (blue), fitted (red), and difference (line below observed and calculated patterns) synchrotron XRD profiles for $\text{Mg}(\text{BH}_4)_2 \cdot 2\text{NH}_3\text{-AB}$ at 298 K. Vertical bars indicate the calculated positions of Bragg peaks for $\text{Mg}(\text{BH}_4)_2 \cdot 2\text{AB}$ and AB phases ($\lambda=0.8264 \text{ \AA}$).

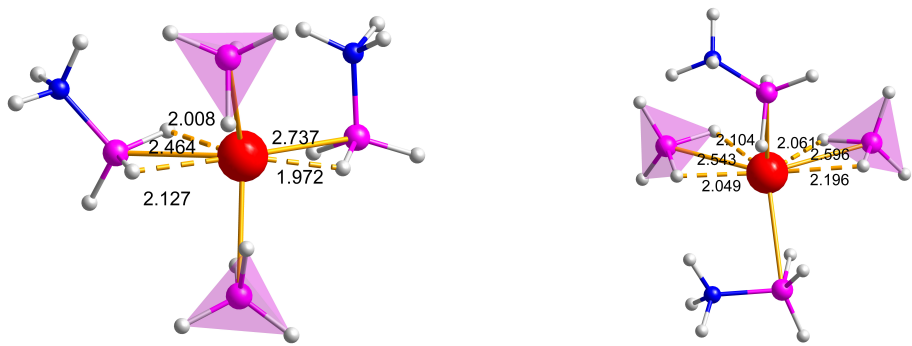


Fig. S3 Molecular structure of complex $\text{Mg}(\text{BH}_4)_2 \cdot 2\text{AB}$. The Mg, B, N and H atoms are represented by red, pink, blue and white spheres, respectively.

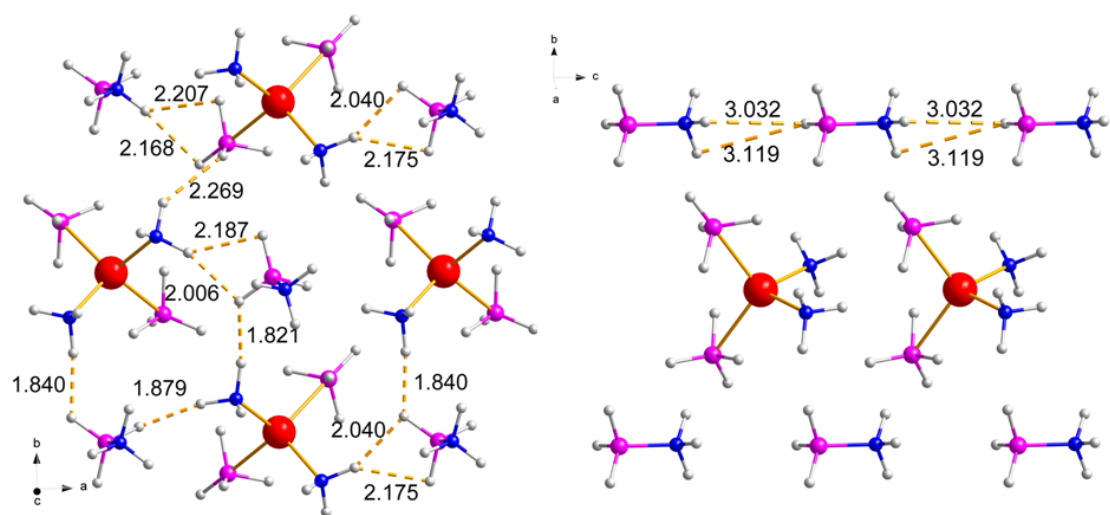


Fig. S4 Schematic diagram of $\text{NH}\cdots\text{HB}$ dihydrogen bonds around NH_3 ligands in $\text{Mg}(\text{BH}_4)_2 \cdot 2\text{NH}_3\text{-AB}$. The Mg, B, N and H atoms are represented by red, pink, blue and white spheres, respectively.

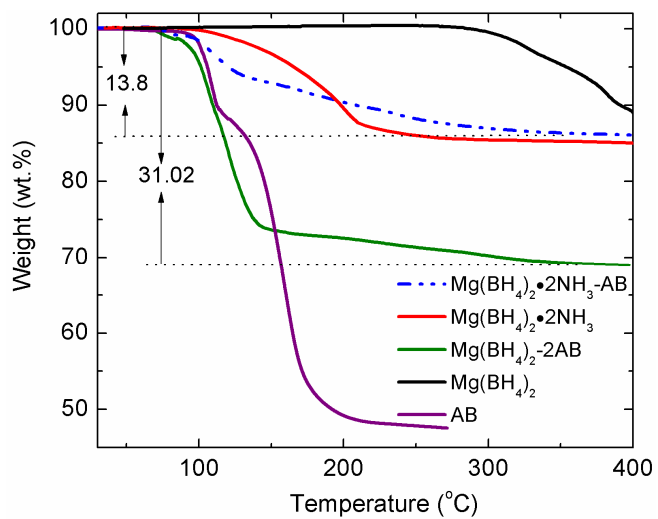


Fig. S5 TGA results of the AB, $\text{Mg}(\text{BH}_4)_2$, $\text{Mg}(\text{BH}_4)_2\text{-2AB}$, $\text{Mg}(\text{BH}_4)_2 \cdot 2\text{NH}_3$ and $\text{Mg}(\text{BH}_4)_2 \cdot 2\text{NH}_3\text{-AB}$ composites with a heating rate of 5 °C/min under 1 atm dynamic N_2 atmosphere.

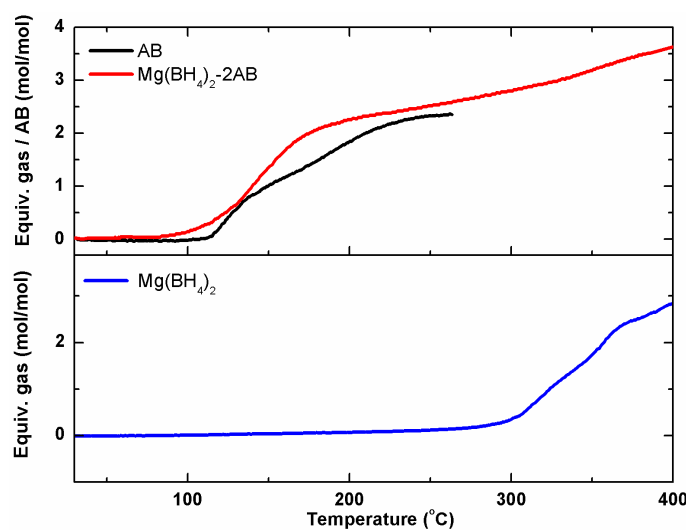


Fig. S6 TPD results for the decomposition of AB and Mg(BH₄)₂-2AB composites with a heating rate of 5 °C/min.

TPD measurements reveal that Mg(BH₄)₂-2AB starts to release hydrogen at ~80 °C and ~2.3 equiv of gas is released by 200 °C, comparable to that of pristine AB. On further heating the sample to 400 °C, a release of additional 1.4 equiv. (4.7 wt%) of pure H₂ is similar to pure Mg(BH₄)₂. These results indicate that the decomposition of Mg(BH₄)₂-2AB in the two regions of RT-200 °C and 200-400 °C is attributed to the decomposition of pure AB and Mg(BH₄)₂, respectively.

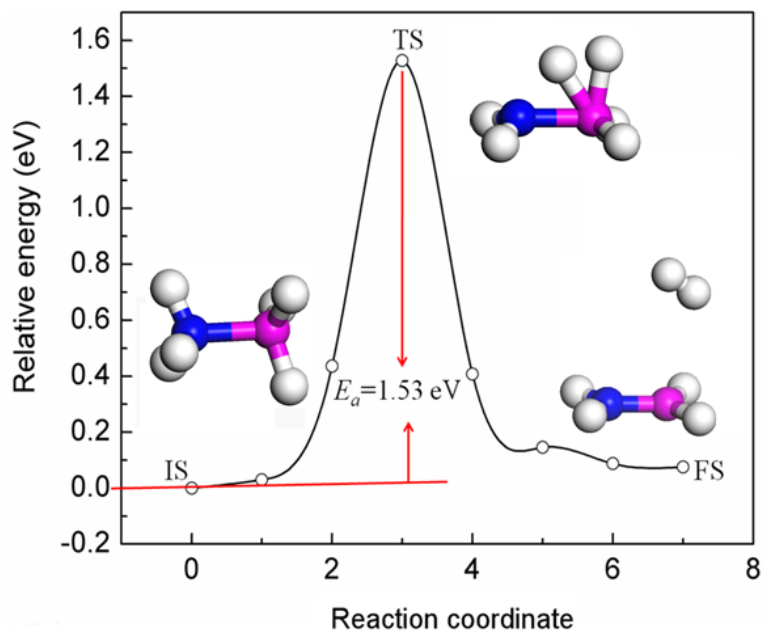


Fig. S7 Energetic profile for the dehydrogenation of pristine AB. Embedded images show the atomic structures of the initial state (IS), transition state (TS), and final state (FS) of the reaction process, respectively. The B, N and H atoms are represented by pink, blue and white spheres, respectively.

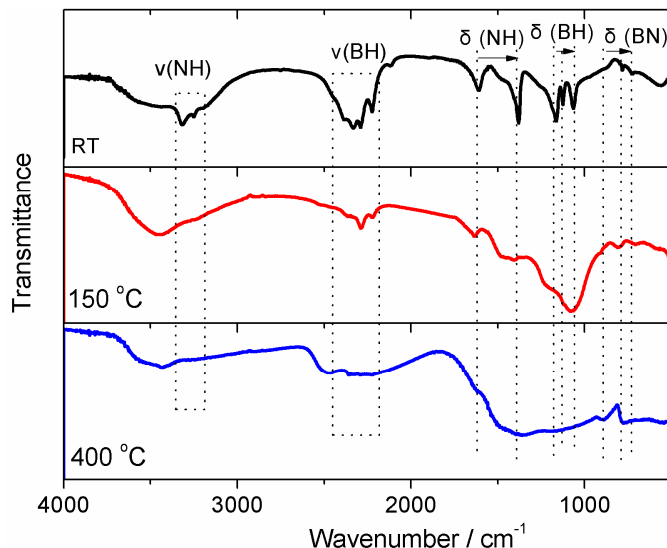


Fig. S8 FTIR spectra for $\text{Mg}(\text{BH}_4)_2\text{-2AB}$ at room temperature and upon heating to 150 and 400 °C, respectively.

The FTIR results in Fig. S8 reveal that, upon heating $\text{Mg}(\text{BH}_4)_2\text{-2AB}$ to 200 °C, the vibrations bands assigned to BH_4 groups were still apparent, meanwhile the peaks belong to N-H vibrations ($3200\text{-}3400 \text{ cm}^{-1}$) and B–H bend mode of AB (1164 cm^{-1}) are diminished, suggesting that the combination of hydridic and protic hydrogen atoms of AB component. On further heating to 400 °C, intensity of the BH groups ($2200\text{-}2400 \text{ cm}^{-1}$) was greatly reduced, indicating the consumption of B–H during the dehydrogenation.

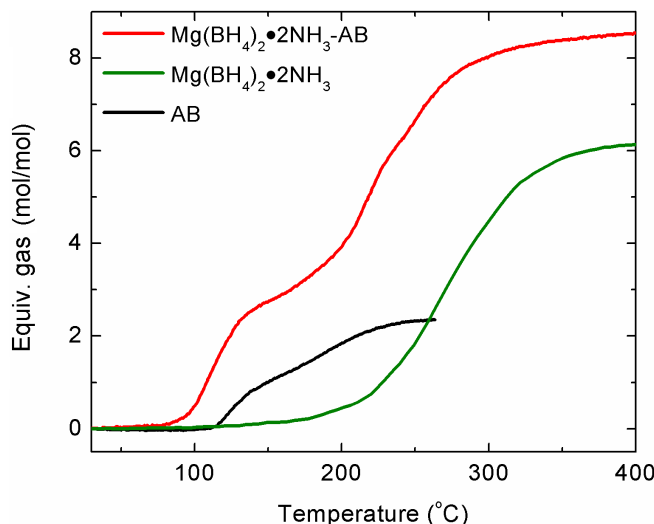


Fig. S9 TPD results for the decomposition of AB, $\text{Mg}(\text{BH}_4)_2 \cdot 2\text{NH}_3$ and $\text{Mg}(\text{BH}_4)_2 \cdot 2\text{NH}_3\text{-AB}$ composites with a heating rate of 5 °C/min.

TPD results show that the AB and $\text{Mg}(\text{BH}_4)_2 \cdot 2\text{NH}_3$ start to release hydrogen at ~100 and 170 °C, and about 1.8 and 0.4 equiv. of gas is released by 200 °C, respectively. Further heating the $\text{Mg}(\text{BH}_4)_2 \cdot 2\text{NH}_3$ to 400 °C results in a release of addition 5.7 equiv. gas, consistent with previous report.² The $\text{Mg}(\text{BH}_4)_2 \cdot 2\text{NH}_3\text{-AB}$ shows a stepwise decomposition with the onset temperature at ~75 °C, and ~4.0 and ~8.5 equiv. of gas is released from $\text{Mg}(\text{BH}_4)_2 \cdot 2\text{NH}_3\text{-AB}$ by 200 and 400 °C, respectively.

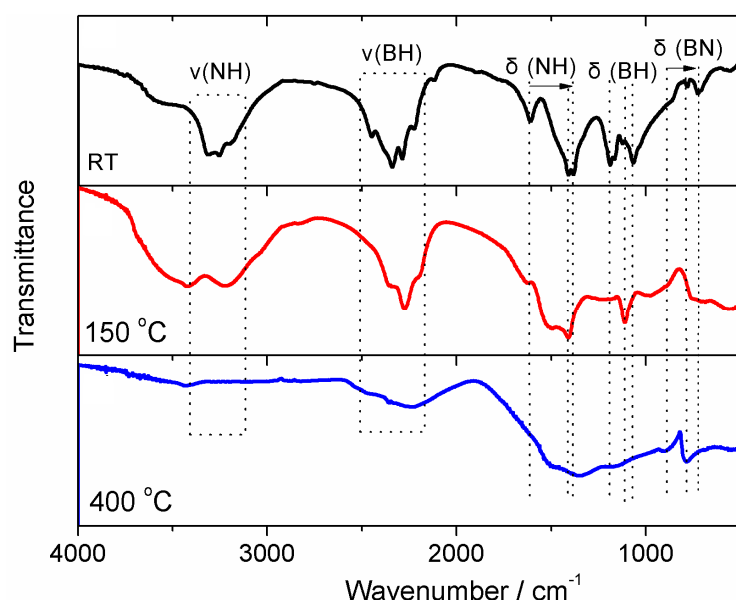


Fig. S10 FTIR spectra for $\text{Mg}(\text{BH}_4)_2 \cdot 2\text{NH}_3\text{-AB}$ at room temperature and upon heating to 150 and 400 °C.

After heating the sample to 150 °C, the vibrations bands assigned to N-H vibrations (3200 and 3400 cm⁻¹) and B-H bend modes of AB (1184 and 1050 cm⁻¹) are diminished, meanwhile the peaks attributed to BH₄ groups were still apparent, suggesting the consumption of B-H bonds in AB and N-H bonds in $\text{Mg}(\text{BH}_4)_2 \cdot 2\text{NH}_3\text{-AB}$. On further heating to 400 °C, after which the dehydrogenation reaction is accomplished, vibrations associated with BH and NH groups almost disappear, along with the appearance of new B-N stretching band located at 890 cm⁻¹, suggesting the consumption of NH and BH groups and formation of BN-like residue during dehydrogenation.

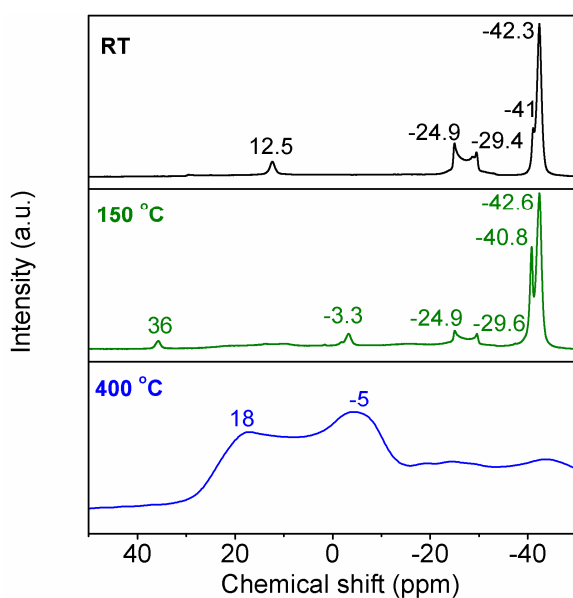


Fig. S11 ^{11}B NMR spectra for $\text{Mg}(\text{BH}_4)_2 \cdot 2\text{NH}_3\text{-AB}$ acquired at different temperatures.

The ^{11}B NMR measurements show that after heat treatment at $150\text{ }^\circ\text{C}$, the relative intensity of resonance peaks corresponding to AB component ($-24.9\text{--}-29.4\text{ ppm}$) decrease, accompanied with the appearance of a new resonance located at -40.8 ppm , which can be assigned to the BH_4^- in $\text{Mg}(\text{BH}_4)_2$, suggesting the consumption of AB and NH_3 molecules during the dehydrogenation.

Table S1. Experimental and crystallographic data of $\text{Mg}(\text{BH}_4)_2 \cdot 2\text{AB}$ and $\text{Mg}(\text{BH}_4)_2 \cdot 2\text{NH}_3\text{-AB}$.

	$\text{Mg}(\text{BH}_4)_2 \cdot 2\text{AB}$	$\text{Mg}(\text{BH}_4)_2 \cdot 2\text{NH}_3\text{-AB}$
<i>Data Collection</i>		
Synchrotron facility	Australian Synchrotron	
Beamline	Powder diffraction	
Wavelength (\AA)	0.8253	0.8264
Detector	Mythen-II	Mythen-II
<i>Unit Cell</i>		
Space group	$P2_12_12_1$	$P4bm$
a	14.4135(2)	9.4643(8)
b	13.2084(2)	9.4643(8)
c	5.1118(1)	5.5229(8)
<i>Refinement</i>		
2 θ range ($^{\circ}2\theta$) used	3.0 – 33.0	3.0 – 45.0
step size ($^{\circ}2\theta$)	0.038	0.038
R_{wp}	0.045	0.056
R_B	0.029	0.041
GoF	1.965	2.136

Table S2. Experimental structural parameters of Mg(BH₄)₂.2AB (Space group $P2_12_12_1$, $a=14.4135(2)$ Å, $b=13.2084(2)$ Å, $c=5.1118(1)$ Å, $V=973.18(2)$ Å³)

Atom	Wyck.	Site	x/a	y/b	z/c
Mg1	4a	1	0.12248	0.76636	0.95973
B11	4a	1	0.51178	0.85805	0.27973
H11a	4a	1	0.52482	0.85676	0.04988
H11b	4a	1	0.44629	0.80596	0.32414
H11c	4a	1	0.58072	0.82896	0.38347
H11d	4a	1	0.49596	0.94227	0.34939
B12	4a	1	0.23325	0.14406	0.29158
H12a	4a	1	0.15671	0.17425	0.33065
H12b	4a	1	0.27041	0.13418	0.49788
H12c	4a	1	0.22708	0.06681	0.17309
H12d	4a	1	0.27508	0.20395	0.16377
B1	4a	1	0.00013	0.88828	0.22133
H1a	4a	1	0.00738	0.85911	0.99444
H1b	4a	1	0.00310	0.81747	0.37505
H1c	4a	1	0.92819	0.93475	0.25442
N2	4a	1	0.08459	0.96213	0.28222
H2a	4a	1	0.09377	0.01570	0.13777
H2b	4a	1	0.07407	0.00253	0.45212
H2c	4a	1	0.14703	0.92414	0.30309
B71	4a	1	0.70953	0.87463	0.84188
H71a	4a	1	0.71033	0.85624	0.07707
H71b	4a	1	0.67316	0.95638	0.79663
H71c	4a	1	0.66882	0.80897	0.72067
N72	4a	1	0.81397	0.87851	0.74187
H72a	4a	1	0.85226	0.81743	0.80618
H72b	4a	1	0.81775	0.87621	0.54063
H72c	4a	1	0.84859	0.94326	0.80136

Table S3. Experimental structural parameters of Mg(BH₄)₂·2NH₃-AB (space group *P4bm*, *a*=9.4643(8) Å, *c*=5.5229(8) Å, V= 494.70(7) Å³)

Atom	Ox.	Wyck.	S.O.F.	x/a	y/b	z/c
Mg1	2b	1	0.5	0	0.58780	
B11	4c	1	0.34667	0.84667	0.33275	
H11a	8d	1	0.25045	0.82552	0.46662	
H11b	8d	1	0.30960	0.93232	0.18836	
N21	4c	1	0.12228	0.62228	0.78818	
H21a	8d	1	0.19685	0.61129	0.66389	
H21b	8d	0.5	0.13286	0.54759	0.91236	
B1	2a	1	0	0	0.90367	
N2	2a	1	0	0	0.19167	
H1a	8d	1	0.11076	0.94064	0.89663	
H1b	8d	0.75	0.10315	0.01729	0.19444	

References

1. G. L. Soloveichik, M. Andrus, Y. Gao, J. C. Zhao and S. Kniajanski, *Int. J. Hydrogen Energy*, 2009, **34**, 2144-2152.
2. G. Soloveichik, J. H. Her, P. W. Stephens, Y. Gao, J. Rijssenbeek, M. Andrus and J. C. Zhao, *Inorg. Chem.*, 2008, **47**, 4290-4298.
3. A. Boultif and D. Louer, *J. Appl. Crystallogr.*, 2004, **37**, 724–731
4. L. Palatinus, and G. Chapuis, *J. Appl. Cryst.*, 2007, **40**, 786-790,
5. Bruker AXS (2008): TOPAS V4.2: General profile and structure analysis software for powder diffraction data. - User's Manual, Bruker AXS, Karlsruhe, Germany.
6. G. Kresse and J. Furthmüller, *Phys. Rev. B*, 1996, **54**, 11169.
7. P. E. Blöchl, *Phys. Rev. B*, 1994, **50**, 17953.
8. J. P. Perdew, K. Burke and Y. Wang, *Phys. Rev. B*, 1996, **54**, 16533-16539.
9. J. P. Perdew, K. Burke and M. Ernzerhof, *Phys. Rev. Lett.*, 1996, **77**, 3865-3868.
10. H. J. Monkhorst and J. D. Pack, *Phys. Rev. B*, 1976, **13**, 5188-5192.
11. S. Grimme, *J. Comput. Chem.*, 2006, **27 (15)**, 1787-1799.
12. G. Henkelman, B. P. Uberuaga and H. Jónsson, *J. Chem. Phys.*, 2000, **113**, 9901.